

OFFICE OF NAVAL RESEARCH

Contract N00014-89-J-1052

R & J Code 4134036

Technical Report No. 49

ON THE FORMATION OF MALEIC ANHYDRIDE ON A VANADYL PYROPHOSPHATE SURFACE:  
A THEORETICAL STUDY OF THE MECHANISM

AD-A222 749

by

B. Schjøtt and K. A. Jørgensen  
Department of Chemistry  
Aarhus University  
DK-8000 Arhus C, Denmark

Roald Hoffmann  
Department of Chemistry and Materials Science Center  
Cornell University  
Ithaca, NY 14853 USA

Prepared for Publication

in

Langmuir

DTIC  
SELECTE  
JUN 03 1990  
E D

Reproduction in whole or in part is permitted  
for any purpose of the United State Government

This document has been approved for public release  
and sale; its distribution is unlimited

**REPORT DOCUMENTATION PAGE**

1a. REPORT SECURITY CLASSIFICATION <b>Unclassified</b>		1b. RESTRICTIVE MARKINGS	
2a. SECURITY CLASSIFICATION AUTHORITY		DISTRIBUTION / AVAILABILITY OF REPORT	
2b. DECLASSIFICATION / DOWNGRADING SCHEDULE			
4. PERFORMING ORGANIZATION REPORT NUMBER(S) <b>#49</b>		5. MONITORING ORGANIZATION REPORT NUMBER(S)	
6a. NAME OF PERFORMING ORGANIZATION <b>Department of Chemistry</b>	6b. OFFICE SYMBOL <i>(if applicable)</i>	7a. NAME OF MONITORING ORGANIZATION <b>ONR</b>	
6c. ADDRESS (City, State, and ZIP Code) <b>Cornell University Baker Laboratory Ithaca, NY 14853-1301</b>		7b. ADDRESS (City, State, and ZIP Code) <b>800 Quincy Street, Arlington, VA</b>	
8a. NAME OF FUNDING / SPONSORING ORGANIZATION <b>Office of Naval Research</b>	8b. OFFICE SYMBOL <i>(if applicable)</i>	9. PROCUREMENT INSTRUMENT IDENTIFICATION NUMBER <b>Report #49</b>	
8c. ADDRESS (City, State, and ZIP Code)		10. SOURCE OF FUNDING NUMBERS	
		PROGRAM ELEMENT NO.	TASK NO.
		PROJECT NO.	WORK UNIT ACCESSION NO.
11. TITLE (Include Security Classification) <b>On the Formation of Maleic Anhydride on a Vanadyl Pyrophosphate Surface. A Theoretical Study of the Mechanism</b>			
12. PERSONAL AUTHOR(S) <b>B. Schjøtt, K. A. Jørgensen and R. Hoffmann</b>			
13a. TYPE OF REPORT <b>Technical Report #49</b>	13b. TIME COVERED FROM _____ TO _____	14. DATE OF REPORT (Year, Month, Day) <b>May 25, 1990</b>	15. PAGE COUNT
16. SUPPLEMENTARY NOTATION			
17. COSATI CODES		18. SUBJECT TERMS (Continue on reverse if necessary and identify by block number)	
FIELD	GROUP	SUB-GROUP	
		maleic anhydride, hydrocarbons, catalysis, DHF <sub>2</sub> , vanadyl pyrophosphate surfaces, oxidation <b>UG</b>	
19. ABSTRACT (Continue on reverse if necessary and identify by block number)			
<p>An analysis of the electronic structure of a vanadyl pyrophosphate surface and of the oxidation of 1,3-butadiene to maleic anhydric by molecular oxygen catalyzed by this surface is presented. The surface contains pairs of edge-sharing vanadium-oxygen octahedra. Each pair has two vanadyl groups, one pointing towards the bulk of the catalyst, the other one being free to interact with incoming molecules. The frontier orbitals of 1,3-butadiene are set up for an interaction with the oxygen in the vanadyl group in a [2+4] like concerted mechanism forming a 2,5-dihydrofuran. The most favourable geometries of the adsorbed species are discussed from an analysis based on the extended Hückel approach.</p> <p>The activation of molecular oxygen on the surface is discussed. A comparison of two structures, <math>\eta^1</math>-superoxo and <math>\eta^2</math>-peroxo adsorbed dioxygen is presented. A mechanism for the oxygen transfer to 2,5-dihydrofuran is proposed involving an initial abstraction of a hydrogen in the 2-position from 2,5-dihydrofuran by the coadsorbed dioxygen species, leading to first a 2-hydroxy derivative followed by the formation of an asymmetric unsaturated lactone. The oxidation of the 5-position is suggested to take place in a similar way.</p>			
20. DISTRIBUTION / AVAILABILITY OF ABSTRACT <input checked="" type="checkbox"/> UNCLASSIFIED/UNLIMITED <input type="checkbox"/> SAME AS RPT. <input type="checkbox"/> DTIC USERS		21. ABSTRACT SECURITY CLASSIFICATION <b>unclassified</b>	
22a. NAME OF RESPONSIBLE INDIVIDUAL <b>Roald Hoffmann</b>		22b. TELEPHONE (Include Area Code) <b>607-255-3419</b>	22c. OFFICE SYMBOL

sta

edak

Hueckel

# On the Formation of Maleic Anhydride on a Vanadyl Pyrophosphate Surface. A Theoretical Study of the Mechanism.

Birgit Schiøtt<sup>a</sup>, Karl Anker Jørgensen<sup>a\*</sup> and Roald Hoffmann<sup>b\*</sup>

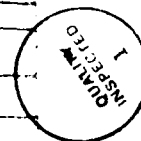
Department of Chemistry, Aarhus University, DK-8000 Århus C, Denmark  
and Department of Chemistry and Materials Science Center, Cornell  
University, Ithaca, N.Y. 14853-1301, USA.

**Abstract:** An analysis of the electronic structure of a vanadyl pyrophosphate surface and of the oxidation of 1,3-butadiene to maleic anhydride by molecular oxygen catalyzed by this surface is presented. The surface contains pairs of edge-sharing vanadium-oxygen octahedra. Each pair has two vanadyl groups, one pointing towards the bulk of the catalyst the other one being free to interact with incoming molecules. The frontier orbitals of 1,3-butadiene are set up for an interaction with the oxygen in the vanadyl group in a [2+4] like concerted mechanism forming a 2,5-dihydrofuran. The most favourable geometries of the adsorbed species are discussed from an analysis based on the extended Hückel approach.

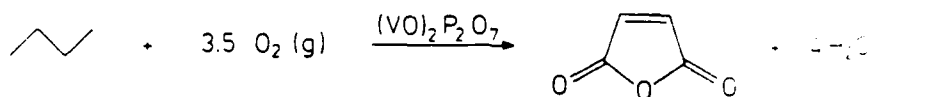
The activation of molecular oxygen on the surface is discussed. A comparison of two structures,  $\eta^1$ -superoxo and  $\eta^2$ -peroxo adsorbed dioxygen is presented. A mechanism for the oxygen transfer to 2,5-dihydrofuran is proposed involving an initial abstraction of a hydrogen in the 2-position from 2,5-dihydrofuran by the coadsorbed dioxygen species, leading to first a 2-hydroxy derivative followed by the formation of an asymmetric unsaturated lactone. The oxidation of the 5-position is suggested to take place in a similar way.

a: Aarhus University  
b: Cornell University

Accession For	
NTIS	<input checked="" type="checkbox"/>
GRA&I	<input checked="" type="checkbox"/>
DTIC TAB	<input type="checkbox"/>
Unannounced	<input type="checkbox"/>
Justification	
By _____	
Distribution/	
Availability Codes	
Dist	Avail and/or Special
A-1	



Understanding and control of the transfer of oxygen and other heteroatoms to and from organic and inorganic species is pursued in academic as well as in industrial research.<sup>1</sup> Among commercially feasible heterogeneously catalyzed reactions, the class of selective oxidations of hydrocarbons is very important. The process of allylic ammoxidation of propylene to acrylonitrile on various mixed metal oxides<sup>2</sup> is an important reaction and 4.3 million tons<sup>3</sup> of the nitrile are so produced per year worldwide. The epoxidation of ethylene to ethylene oxide on a silver surface<sup>4</sup> is also very used in the industry (5.8 million tons per year<sup>3</sup>). Generally, for these very important and useful reactions the underlying mechanisms of the selective oxidations are not well understood. Some theoretical investigations of acrolein production from propylene using a mixed molybdenum-bismuth-oxide catalyst<sup>5</sup> and for the adsorption of ammonia on V<sub>2</sub>O<sub>5</sub>, an important step in the ammoxidation reaction,<sup>2c</sup> have been published. A study of ethylene epoxidation on a Ag(110) surface<sup>6</sup> has also appeared recently. Perhaps the most intriguing process among the heterogeneously catalyzed selective oxidation reactions is the synthesis of maleic anhydride from *n*-butane over a vanadium phosphorous oxide surface in the presence of molecular oxygen [equation (1)].<sup>7</sup>

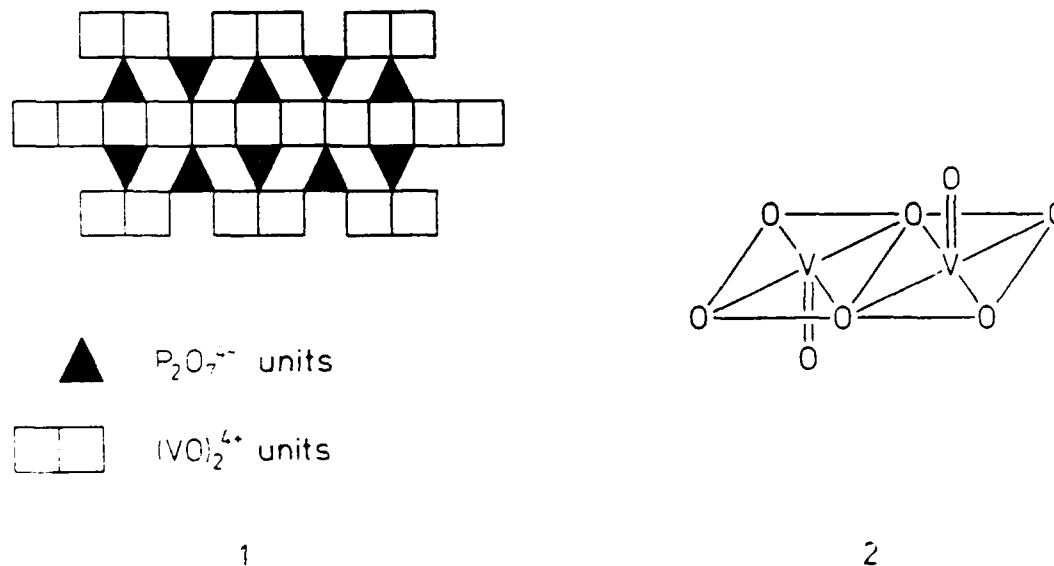


This reaction, being a 14-electron oxidation involving an abstraction of eight hydrogen atoms and an insertion of three oxygen atoms, has been the subject of a large number of reports<sup>7,8</sup> and will be the matter discussed in this paper.

The solid state chemistry of the vanadium phosphorous oxide system is characterized by a large number of crystalline phases<sup>9</sup> that easily interconvert upon reduction and oxidation.<sup>7a,10</sup> The active vanadium phosphorous oxide phase in the oxidation of *n*-butane has been disputed in the literature.<sup>7a,9,10</sup> Generally, it is agreed that the presence of the vanadyl pyrophosphate phase, (VO)<sub>2</sub>P<sub>2</sub>O<sub>7</sub>, in the catalyst is necessary for the

reaction to proceed.<sup>11</sup> An analysis of a commercially used vanadium phosphorous oxide catalyst showed only the presence of one crystalline phase by X-ray diffraction measurements, namely the vanadyl pyrophosphate phase.<sup>7a</sup> Furthermore, it revealed an oxidation state for vanadium of 4.00-4.03 and a P:V ratio of  $1.00 \pm 0.02$ ,<sup>7a</sup> consistent with the assignment of  $(VO)_2P_2O_7$  as the active phase. Most of the mechanistic studies are thus performed using a clean vanadyl pyrophosphate surface as the catalyst. Here also we will concentrate on this particular vanadium phosphorous oxide structure.

Vanadyl pyrophosphate has a layered structure. The layers consist of pairs of edge-sharing vanadium-oxygen octahedra linked together in the plane by pyrophosphate units, 1. The planes are linked together through the axial oxygens of the edge-sharing octahedra. A tetragonal distortion of the octahedral environment of vanadium in the double chain direction is observed by the X-ray crystallographic investigations.<sup>12</sup> The two vanadyl groups hereby formed are placed *trans* to one another within one pair of edge-sharing vanadium octahedra, 2. The interlayer bonding can be described as a weak Lewis acid  $\rightarrow$  Lewis base interaction ( $V=O \cdots \rightarrow V=O$ ).<sup>8a</sup>



It is very important to obtain knowledge of the surface chemical structure of  $(VO)_2P_2O_7$  in order to trace a likely mechanism for the selective oxidation of *n*-butane to maleic anhydride. Satsuma *et al.* have described the surface structure in terms of the number of surface  $V=O$  groups and

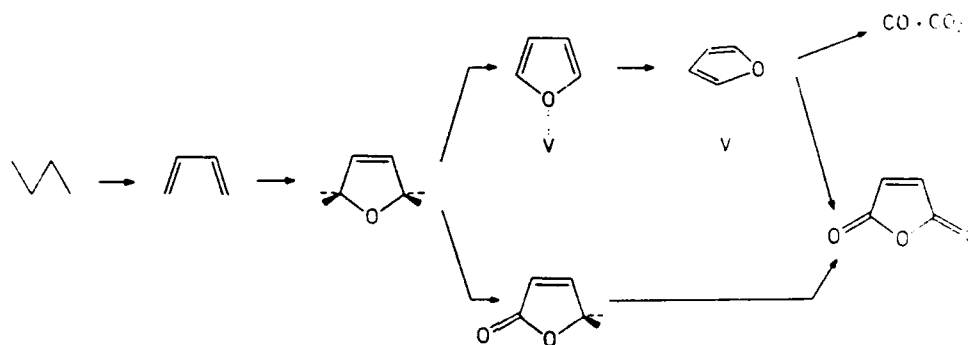
surface acid sites, using various physical and chemical methods.<sup>13</sup> They were able to show that the vanadyl group, V=O, is presented to a large extent on the surface of vanadyl pyrophosphate. The surface acid sites were identified as Brønsted acid sites, such as P-OH, whereas a small number of Lewis acid sites were found associated to the surface vanadium atoms. In this study we will apply one layer of the vanadyl pyrophosphate structure as a model for the active surface. One vanadyl dimer contains both the surface V=O unit as well as a Lewis acid site, namely at the vanadyl group pointing towards the bulk.

The rate-determining step in the oxidation of butane on a vanadyl pyrophosphate surface has been shown to be the activation of the methylene carbon-hydrogen bond(s).<sup>8a,14</sup> In order to trace the steps of the reaction that are responsible for the large selectivity to maleic anhydride, the oxidation of the thereby formed unsaturated species, such as 1-butene and 1,3-butadiene has been very intensively studied.<sup>11c,15</sup> For these species the rate-controlling step towards maleic anhydride is the insertion of oxygen into the hydrocarbon.<sup>15a</sup> This is very different from other olefinic selective oxidations, as for example the propylene to acrolein synthesis.<sup>2</sup>

Concerning the oxygen source for the maleic anhydride reaction, it also differs from other selective oxidation reactions. Usually, the bulk of the catalyst is involved in the oxidation of the organic fragment by undergoing a reduction in the promotion of oxygen to the active surface.<sup>16</sup> In the formation of acrolein from propylene on a mixed molybdenum-bismuth-oxide surface the availability of gas-phase oxygen is not an absolute need.<sup>2,17</sup> For this reaction it has been shown by labelling studies that bulk oxygen atoms are transferred to the hydrocarbon.<sup>17</sup> In the case of vanadyl pyrophosphate bulk oxygens are not involved in the reaction<sup>18</sup> and only small amounts of maleic anhydride are formed in the absence of O<sub>2</sub>(g).<sup>7a,8a,b</sup> The main product of 1-butene oxidation was thus crotonaldehyde, obtained by an oxy-dehydrogenation and an allylic oxidation.<sup>15b</sup>

How the molecular oxygen becomes activated at the vanadyl pyrophosphate surface, and in which form (gas-phase, physisorbed or surface-lattice) it becomes incorporated into the products, is still an unanswered and disputed question.<sup>7,8</sup> It has been rationalized that the

vanadyl pyrophosphate surface can adsorb one oxygen molecule per two surface vanadium atoms.<sup>8a</sup> Also, by using butadiene as starting material Centi and Trifirò were able to show that the furan-oxygen is introduced through an attack of an electrophilic oxygen on the 1,4-positions of butadiene to give 2,5-dihydrofuran.<sup>15a</sup> Recently, Busca and Centi<sup>8b</sup> detected at least three different intermediates besides the 2,5-dihydrofuran, namely an unsaturated lactone and two structures of adsorbed furan. Two competing reaction paths could be distinguished, as shown in Scheme 1. There is postulated a fast path, involving an asymmetric unsaturated lactone (lower reaction path) and a slower one, passing through a furan intermediate (upper reaction path). The slow path was shown to be the less selective way, giving rise to the formation of CO and CO<sub>2</sub>.<sup>8b</sup>

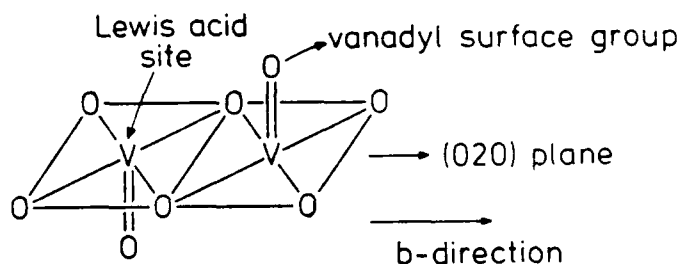


Scheme 1

In this study we will focus on the lower more selective path. The "upstanding" O-coordinated form of adsorbed furan is more stable by ~2-3 eV than the "lying down"  $\pi$ -coordinated form, depicted in the upper path. An analysis of the bonding situation between a vanadyl pyrophosphate surface and the various adsorbates (butadiene, 2,5-dihydrofuran and the lactone) is made in order to trace the most likely adsorption geometry of these intermediates. The nature of the active oxygen is also discussed and a mechanism for the selective oxygen transfer is proposed. Throughout the study the extended Hückel<sup>19</sup> approximation is used. Due to limitations in computational time a cluster model is applied for the more complex structures; otherwise tight binding<sup>20</sup> calculations are performed. Further details of the calculations are given in the Appendix.

## The Surface of Vanadyl Pyrophosphate.

Let us start with an analysis of the clean vanadyl pyrophosphate surface. Although the structure of the surface is disputed in the literature<sup>7a,9,10</sup> we will here limit ourselves to the (020) plane of  $(VO)_2P_2O_7$  as the active surface.<sup>7a,14</sup> It has been proposed that the active sites are located at interfaces between different crystal phases.<sup>9c</sup> Though a crystal of one phase only, the vanadyl pyrophosphate phase serves well as a catalyst for the selective oxidation of *n*-butane to maleic anhydride.<sup>8</sup> Surface sensitive experiments conclude that vanadyl,  $V=O$ , sites are found at the surface of a  $(VO)_2P_2O_7$  crystal and also that surface Lewis acid sites are found.<sup>13</sup> One pair of edge-sharing  $VO_5$  units contains both of these functional groups, 3.



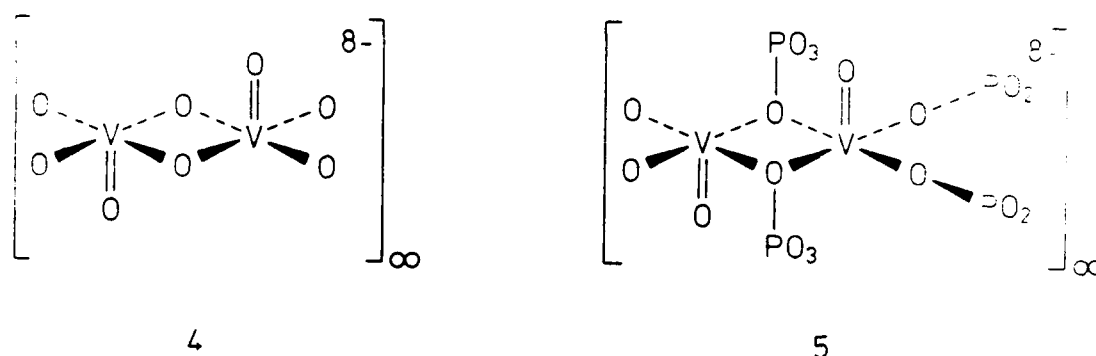
3

The surface of  $V_2O_5$  has been analyzed theoretically.<sup>2c</sup> The structure of  $V_2O_5$  consists also of tetragonally distorted edge-sharing octahedra. Because of the highly ionic structures for  $V_2O_5$  and  $(VO)_2P_2O_7$  the bonding within both structures is relatively localized. Though differences in the properties of the surface layers are computed.<sup>2c,13</sup>

Due to limitations in computational time we will only use one layer of the vanadyl pyrophosphate structure as a model for the active surface. Usually, in the case of metal single crystal surfaces three layers or more are recommended,<sup>21</sup> but for more ionically bonded, therefore localized, systems a one layer model has been applied successfully as *e.g.* in the analysis of the adsorption of organo-rhodium compounds on a rutile surface.<sup>22</sup> The unit



cell within one (020) plane of vanadyl pyrophosphate is rather large, due to the alternating orientations of the pyrophosphate,  $P_2O_7^{4-}$ , groups. To avoid this enormous unit cell we make a one-dimensional approximation. In the following we will compare characteristic features of two one-dimensional chains made from pairs of edge-sharing  $VO_5$  units. The dimension taken into account is the one along the b-direction of the unit cell, meaning along the direction of the edge-sharing vanadyl groups. The first model consists of the bare vanadyl units, 4. The second structure applied attaches  $PO_3$  units as models for the pyrophosphates, 5. The charge of each structural unit is chosen so as to give vanadium an oxidation state of +4 (all oxygens are in the -2 oxidation state).



Small defects in the  $(VO)_2P_2O_7$  structure give rise to a small quantity of  $V^{5+}$  centers.<sup>7a</sup> Some authors have attributed to these the large selectivity for maleic anhydride.<sup>7,15b,23</sup> A calculation with vanadium in the oxidation state +5 is thus performed in order to investigate how the oxidation state can influence the adsorption processes regarded.

The distance between two nearest oxygens from two neighbouring unit cells is rather large (the average oxygen-oxygen separation within a pyrophosphate unit is  $2.50\text{\AA}$ <sup>12</sup>) so we expect very little inter unit cell interactions. For this reason we did calculations on the parent compounds to the two chains. A calculation with  $P(OH)_3$  units as models for the pyrophosphates, 6, was also carried out for the +4 oxidation state of vanadium.

Important results are listed in Table 1 for the calculations with vanadium in a +4 oxidation state and in Table 2 for an oxidation state of +5.

---

Table 1

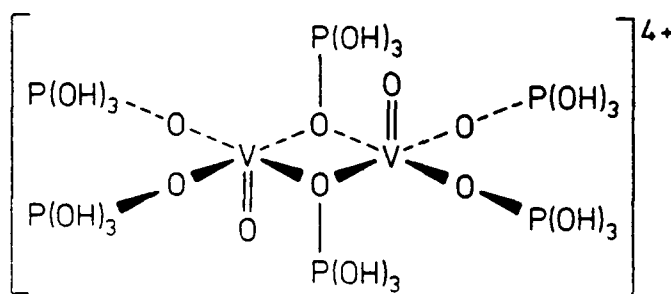
---



---

Table 2

---



6

For both oxidation states considered the different models used gives consistent results. For the set of calculations with vanadium in the +4 oxidation state all models give a net charge on vanadium of approximately +2.0 and of -1.26 for the double bound oxygens. Also, the vanadium-vanadium (V-V) overlap population is computed to be small and positive in all models. The overlap population of the vanadium-oxygen double bond is also almost unchanged from one model to the other, varying from 0.758 to 0.771.

The other set of calculations with two electrons less, giving vanadium in the +5 oxidation state, also comes out with consistent numbers for the characteristics listed. The charge on vanadium is about +3.0 in all three models. The overlap population of the vanadium-oxygen double bond remains unchanged compared to the calculations for the +4 oxidation state.

8

**Table 1.** Electronic properties for the different models used for the vandy pyrophosphate surfaces with vanadium in a +4 oxidation state.

Charge on V	1.95	2.03	2.03	2.14	2.20
Charge on double bound O	-1.26	-1.26	-1.26	-1.26	-1.26
Average charge of P	-	2.63	-	2.69	2.60
<u>Overlap populations</u>					
V - V	0.010	0.039	0.010	0.041	0.042
V = O	0.758	0.767	0.761	0.773	0.771

Table 2. Electronic properties for different the models used for the vanadyl pyrophosphate surface with vanadium in a +5 oxidation state.

Charge on V	2.92	3.01	2.91
Charge on double bound O	-1.26	-1.26	-1.26
Average charge of P	-	2.63	-
<u>Overlap populations</u>			
V - V	-0.037	0.039	0.010
V = O	0.758	0.767	0.761

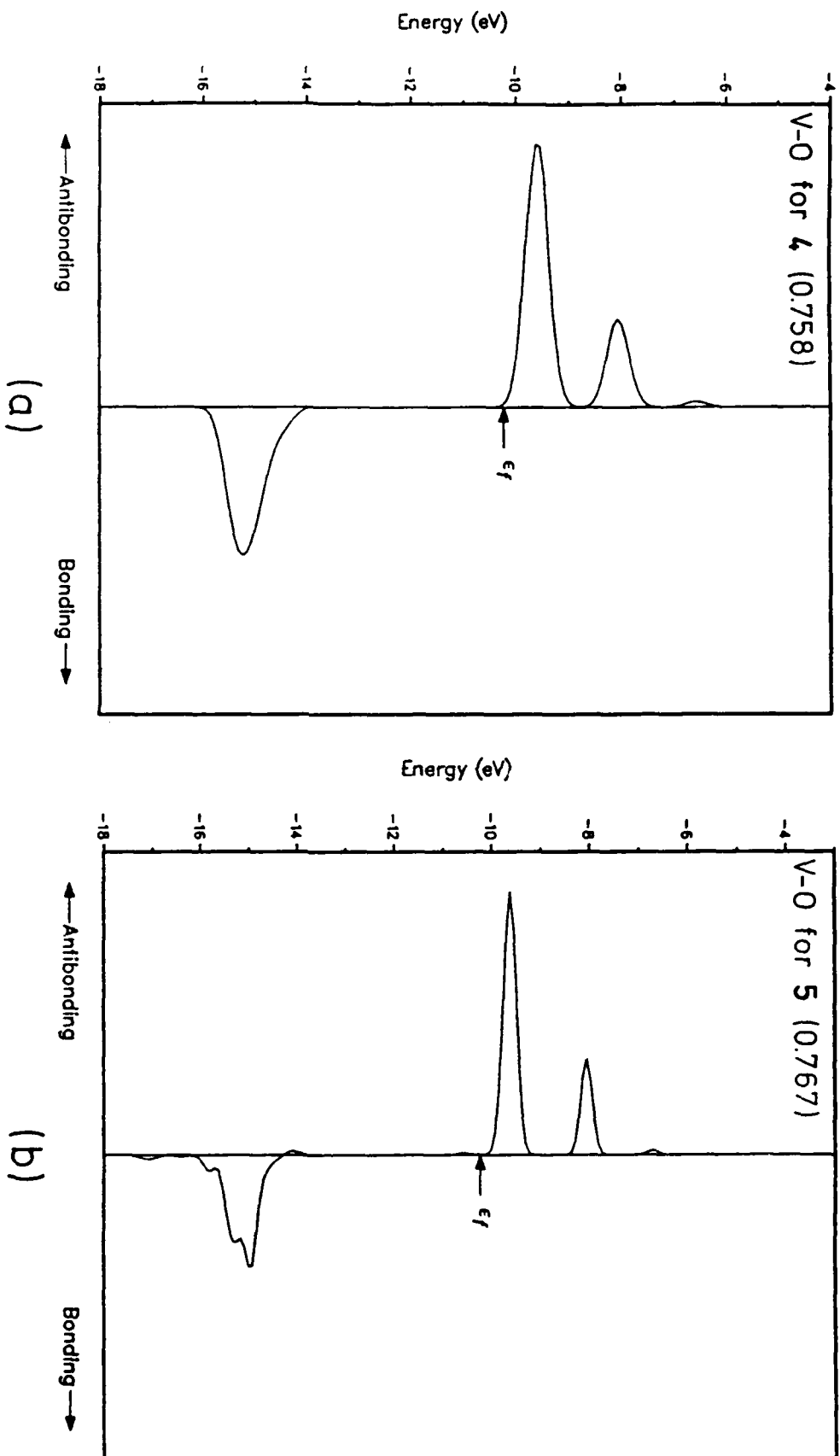


Figure 1: Crystal Orbital Overlap Population (COOP) for the V=O bond in 4 (a) and 5 (b).

The V-V overlap population has now settled on a small negative value.

The consistency between the models used is also found in the  $V=O$  COOP<sup>24</sup> (Crystal Orbital Overlap Population) curves for 4 and 5, as seen in Figure 1 (a) and (b), respectively. Both have a bonding peak at  $\sim -15$  eV and two peaks contributed by orbitals with antibonding  $V=O$  character above the Fermi level at  $\sim -9.5$  eV and  $-8.0$  eV. The fine structure of the peaks is different because of the changed environment, but the main features remain the same. We will discuss below the origin of these features.

---

Figure 1

---

The removal of two electrons from the system by going from the +4 oxidation state of vanadium to the +5 oxidation state is accompanied by a decrease in the small V-V overlap population and an increase in positive charge located on each vanadium. These observations can be rationalized by an analysis of some DOS<sup>24</sup> (Density of States) and COOP curves. Some plots for structure 5 is shown in Figure 2 to explain the sign and magnitude of the V-V overlap population calculated.

---

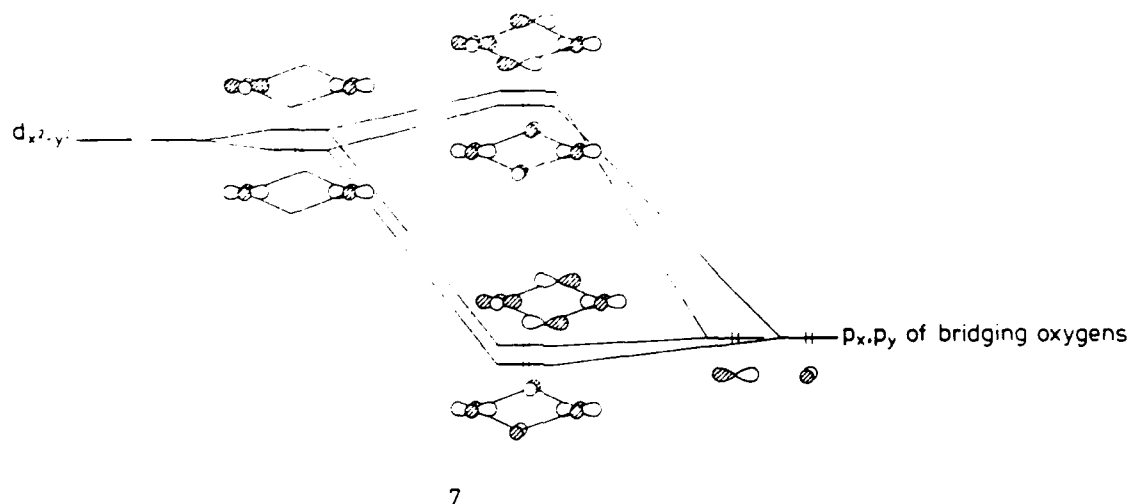
Figure 2

---

The Fermi level of 5 is located at  $-10.2$  eV. The plot shown in Figure 2 (a) is the contribution from the vanadium  $d_{x^2-y^2}$  orbitals to the total DOS. We see that  $\sim 10\%$  of the states are found in the  $-14.5$  eV to  $-17.0$  eV range. These states cause a bonding and an antibonding peak in the V-V COOP curve, as depicted in Figure 2 (b). The antibonding peak is larger in magnitude than the bonding one, so the total V-V overlap population contributed by these lower peaks is negative, as calculated for the +5 oxidation state structures. The major part (90%) of the  $d_{x^2-y^2}$  states is located around the Fermi level. These states also create a bonding and an antibonding V-V peak in the COOP. The Fermi level cuts at an energy half way through this bonding peak explaining the small positive overlap population. This indicates only a small coupling of the d electron located at each vanadium center in agreement with the identification of a triplet

ground state by EPR measurements.<sup>8a</sup> By going to the +5 oxidation state of vanadium two electrons are removed from each structural unit. A loss of 0.96 electrons for each  $d_{x^2-y^2}$  is computed. The Fermi level, located at -10.7 eV, is now far below the upper V-V bonding peak, justifying the decrease in V-V overlap population.

The appearance of two peaks in the DOS for  $d_{x^2-y^2}$  is a consequence of mixing with the p orbitals of the bridging oxygens. The DOS for  $p_x$  and  $p_y$  are plotted in Figure 2 (c) and (d). We see a large contribution in the -14.0 eV to -17.5 eV range and a smaller one (~5%) around the Fermi level. A schematic drawing of the interaction of  $d_{x^2-y^2}$  with the  $p_x$  and  $p_y$  of the bridging oxygens is shown in 7. The  $d_{x^2-y^2}$  orbitals of two vanadiums interact weakly giving a bonding and an antibonding combination. Each of these interact with the p orbital of the bridging oxygens with the right symmetry. The four combinations obtained explain the variations observed in the V-V COOP curve.



The bonding and antibonding combinations of the vanadium  $d_{xy}$  orbitals interact in a similar way with  $p_x$  and  $p_y$  of the bridging oxygens. The DOS for  $d_{xy}$  is plotted in Figure 2 (e). Two major peaks are found above the Fermi level at -5.0 eV and -6.8 eV. These are seen in the V-V

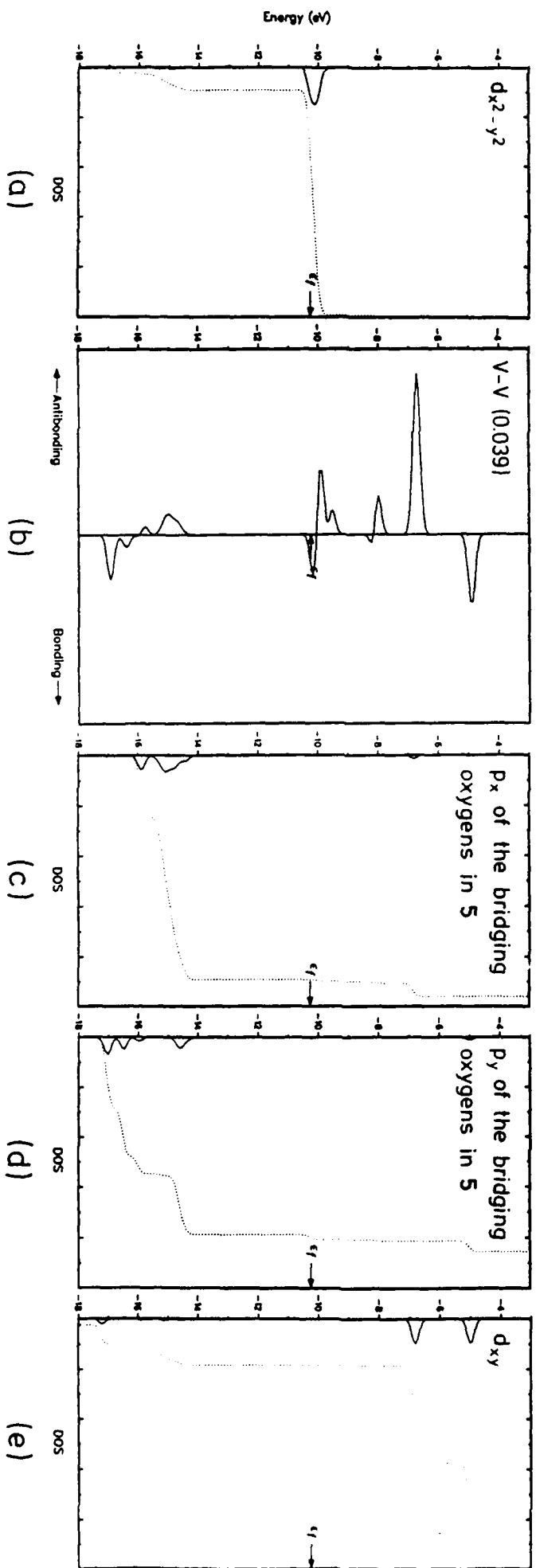
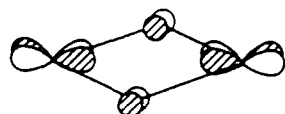
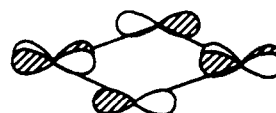


Figure 2: Some projected density of states (DOS) for structure 5. (a) Contribution from the vanadium  $d_{x^2-y^2}$  orbital to the total density of states. (b) Vanadium-vanadium COOP curve. (c) Contribution from the  $p_x$  orbitals of the bridging oxygens. (d)  $p_y$  orbitals of the bridging oxygens. (e) The projected density of states of the vanadium  $d_{xy}$  orbitals. Dotted lines give the integration of the depicted orbital.





8



9

COOP (Figure 2b) as a bonding, 8, and an antibonding peak, 9.

Figure 3 displays some important plots for the understanding of the vanadium-oxygen double bond. Figure 1 (b) showed the COOP of the bond in question. Bonding states are found from -14 eV to -16 eV and the antibonding states are located above the Fermi level with two major peaks at -9.5 eV and -8.0 eV. The vanadium orbitals involved in this bonding are

---

Figure 3

---

depicted in Figure 3 (a) ( $d_{z^2}$ ) and in Figure 3 (b) ( $d_{xz}$ ,  $d_{yz}$ ). The bonding states are made up of interactions of  $d_{xz}$  and  $d_{yz}$  on the metals with  $p_x$  and  $p_y$  of the oxygens and of  $d_{z^2}$  with oxygen  $p_z$  and  $s$ . The antibonding peaks are easily distinguished with help from the DOS's. In Figure 3 (b) the -10.0 eV peak just above the Fermi level is the antibonding  $\pi$  type interaction, 10, whereas the stronger  $\sigma$  interaction has its antibonding peak at a higher energy, -8.0 eV, 11 (Figure 3(a)). No vanadium-oxygen states, bonding or antibonding, are located right below the Fermi level explaining the unaffected V=O overlap population when the oxidation state of vanadium is changed.

The results of these one-dimensional calculations are fully consistent with the picture obtained from calculations on the parent clusters. For the more complex structures where it is harder to resolve the DOS's and COOP's we will therefore use clusters as models for the surface.

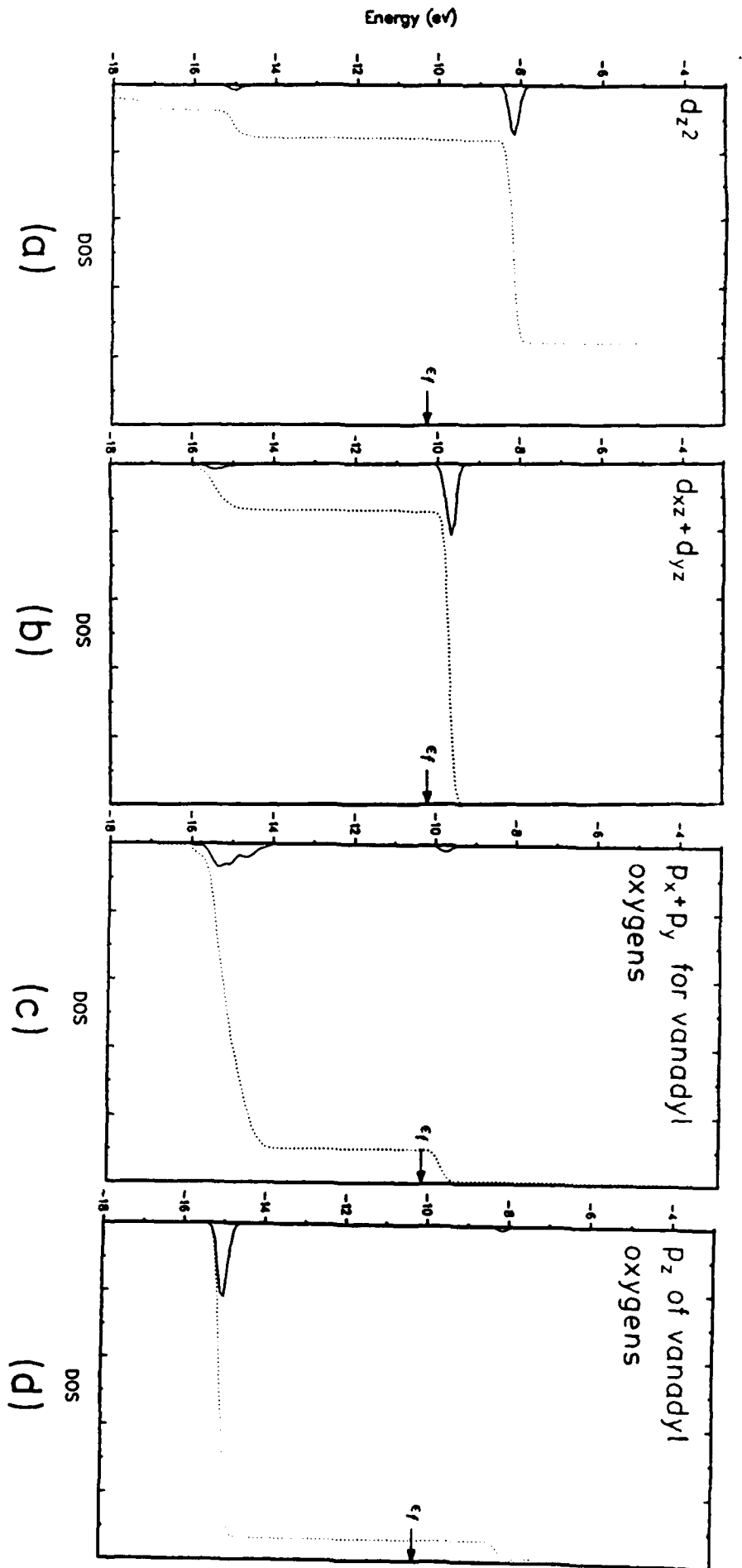
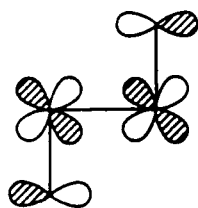
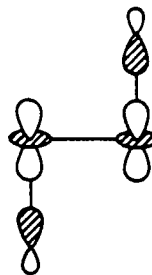


Figure 3: Projected density of states illustrating the V=O bonds in 5. (a) Projected density of states of the vanadium  $d_{z^2}$  orbitals. (b) Contribution of the vanadium  $d_{xz}$  and  $d_{yz}$  orbitals to the total DOS. (c) Projected density of states of  $p_x$  and  $p_y$  from the vanadyl oxygens. (d)  $p_z$  of the vanadyl oxygens. Dotted curves give the integration of the projected DOS.



10



11

In the following we will focus on the oxygen transfer from the vanadyl pyrophosphate surface to butadiene. The hydrogen activation and abstraction steps going from *n*-butane to butadiene will not be considered in this study. Experimentally it is believed that butadiene and *n*-butane pass through the same intermediates on the way to maleic anhydride, the first intermediate being 2,5-dihydrofuran.<sup>7a,8</sup>

### The formation and bonding of 2,5-dihydrofuran.

It has been proposed that the furan oxygen is introduced through an attack of an electrophilic oxygen at the 1,4-positions of butadiene.<sup>15a</sup> This statement is in agreement with a simple orbital interaction diagram between the V=O group of the  $(VO)_2O_6^{8-}$  cluster and butadiene, as shown in Figure 4. The oxygen-carbon distance is set to 1.60 Å and the 1,4-positions of butadiene are at the same x-coordinate as the V=O unit of the surface. The left-hand side shows the frontier orbitals of  $(VO)_2O_6^{8-}$ . We recognize the bonding and antibonding combinations of the vanadium  $d_{x^2-y^2}$  orbitals as the HOMO and LUMO, nearly degenerate in this molecular calculation. Right above the LUMO are located antibonding combinations of  $d_{xz}$  and  $d_{yz}$  with  $p_x$  and  $p_y$ , as in the one-dimensional calculations. These V-O antibonding orbitals are electrophilic in character when interacting with the HOMO of butadiene.

---

Figure 4

---

A decrease in overlap population for the vanadium-oxygen double bond from 0.761 to 0.495 is computed, verifying that a substantial fraction of V=O antibonding orbitals becomes populated upon adsorption. A decrease in overlap population for the carbon carbon double bonds after adsorption is seen too, from 1.465 to 1.137, due to a depletion of 0.67 electrons from the HOMO and a donation of 0.19 electrons to the LUMO of butadiene. A vertically oriented butadiene is also suitable for interaction with the vanadyl oxygen, but the energy of the product is disfavored by ~3 eV compared to the geometry shown in the center of Figure 4. The product of this [4+2] type reaction rearranges to the 2,5-dihydrofuran structure. We have examined some different orientations of 2,5-dihydrofuran (DHF) in order to trace a likely orientation of the intermediate in the maleic anhydride synthesis. Four orientations of DHF adsorbed on a  $(VO)_2O_6^{8-}$  cluster were tried. Two calculations with the DHF ring oriented parallel to the surface, 12, and two calculations with the DHF ring perpendicular to the

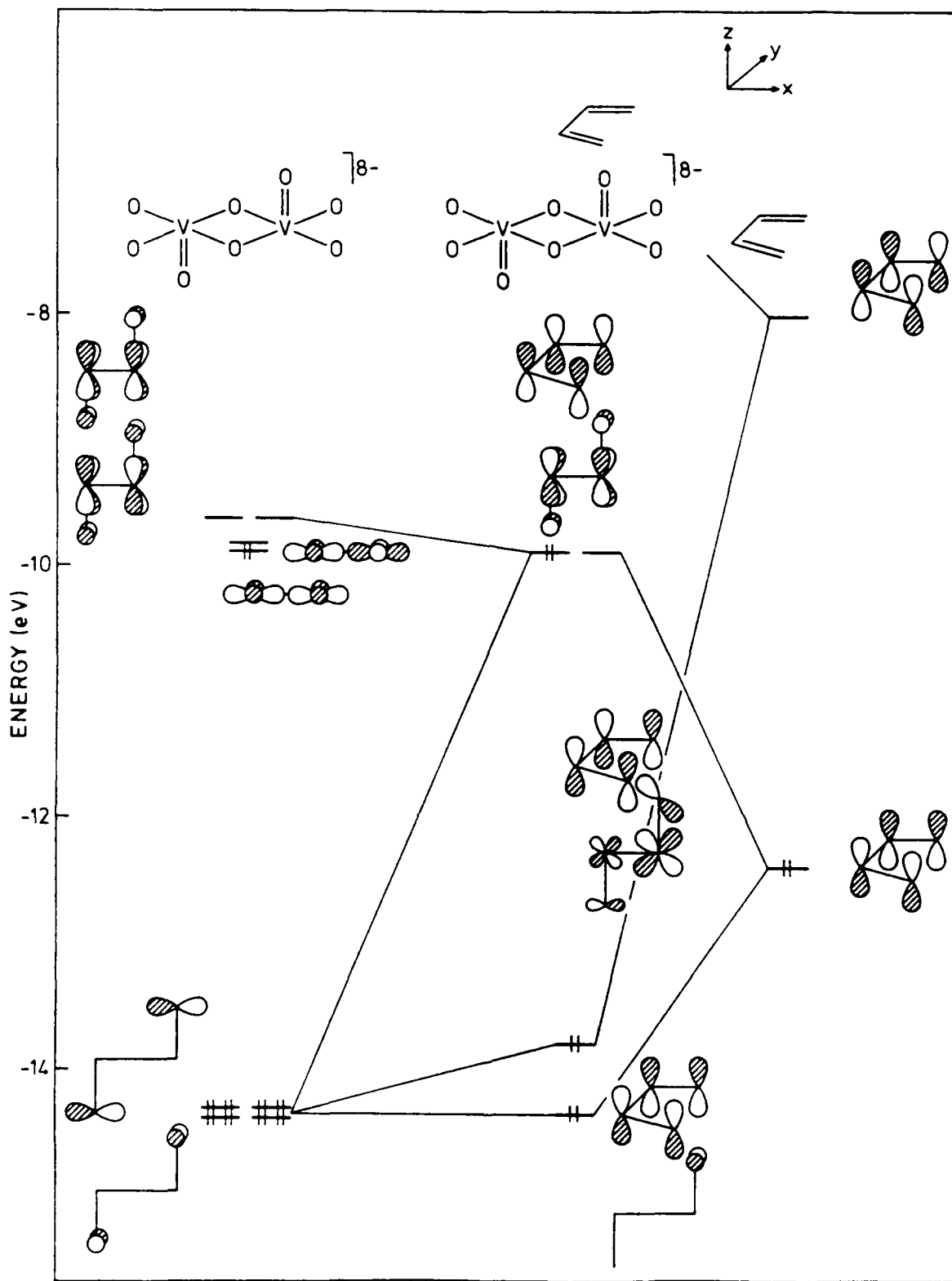
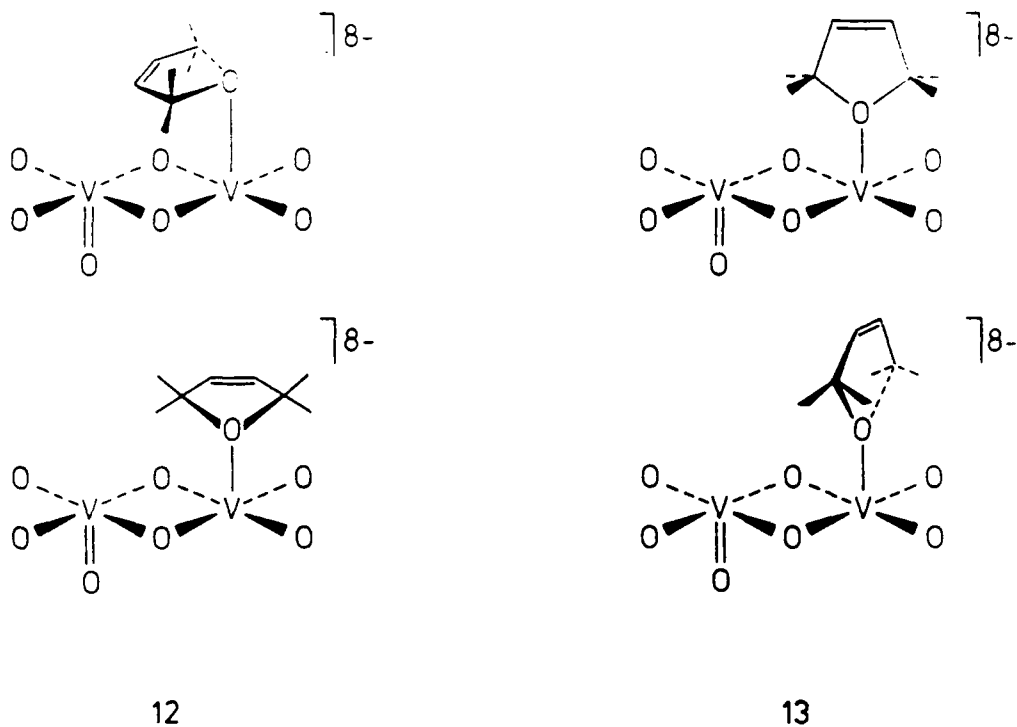


Figure 4: Interaction diagram for an interaction of a  $V_2O_8^{8-}$  fragment (to the left) with 1,3-butadiene (to the right).

surface plane, 13, were carried out. From an energetic point of view the two structures 12 are disfavored by 7 and 9 eV, respectively, compared to 13, and they will not be considered further in this study. The two "upstanding" forms give similar energies. Calculations for these structures were carried out on the simple one-dimensional surface, 5, to reveal whether or not a



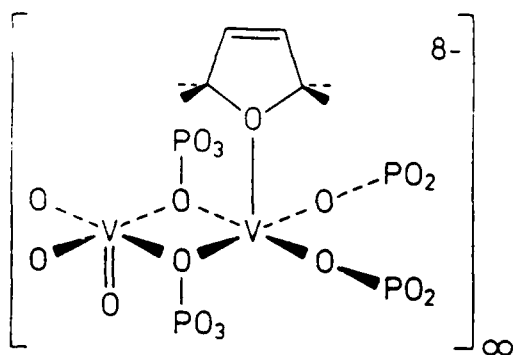
preference in the orientation of DHF could be found. Table 3 lists some results for the two structures examined, 14 and 15. Very similar numbers are computed, though the structure with the ring along the V-V direction, 14, is slightly more favourable by 0.3 eV.

---

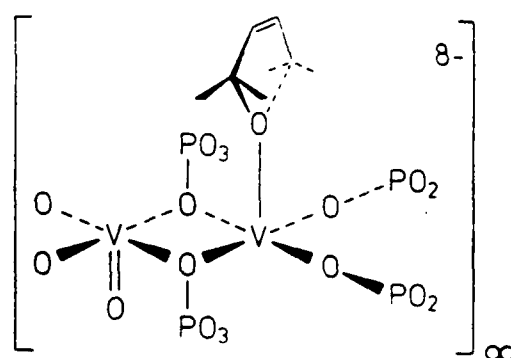
Table 3

---

From these calculations it is concluded that DHF on a vanadyl pyrophosphate surface takes an upright position, but no specific conformation for this orientation can be picked as the most favourable.



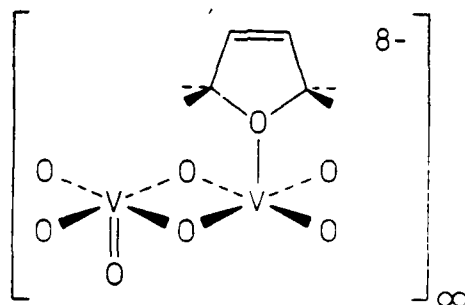
14



15

Let us now proceed to a description of the bonding situation between DHF and the vanadyl pyrophosphate surface. For this purpose a one-dimensional chain of  $(VO)_2O_6^{8-}$  is applied. The distance between the oxygen of DHF and vanadium is arbitrarily set to  $2.0 \text{ \AA}$ .<sup>25</sup> Figure 5 displays some plots to examine the V-O and the C-O bonds of 16. Figure 5 (a) is the

Figure 5



16

COOP curve for the V-O bond. Compared to Figure 1 (a) especially the bonding part has changed by splitting into many separated peaks. The orbitals that make up the five bonding V=O peaks also have either O-C bonding or antibonding character as seen from the O-C COOP in Figure

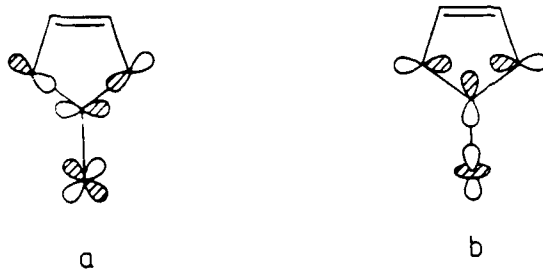
15

Table 3. Total energies and some overlap populations for 14 and 15.

	14	15
Total energy	-3253.1eV	-3252.8eV
<u>Overlap populations</u>		
V = O	0.761	0.762
V - O <sub>DHF</sub>	0.310	0.306
C-O	0.495	0.495



5 (b). The DOS curves (not shown here) reveal that the four smallest (in amplitude) occupied peaks in the two COOP curves are made up from an interaction of the low lying V-O  $\pi_y$  orbitals with the  $p_y$  on the 2,5-carbons of DHF. The two lower peaks are the bonding combinations and the upper ones are the antibonding ones resulting in no net  $\pi$  type bonding between oxygen and carbon in the DHF ring, 17 a. The major peak around  $\sim -15$  eV consists of the  $\sigma$  type bonding orbitals, 17 b. The corresponding antibonding orbitals are located above the Fermi level. Again, the orbital picture obtained from a one-dimensional calculation is consistent with the cluster calculation. From Figure 5 (a) it is seen that the Fermi level cuts at an energy half way through a strongly antibonding V-O band. For the structure with two electrons less, vanadium in the +5 oxidation state, a higher V-O overlap population is thus calculated.



17

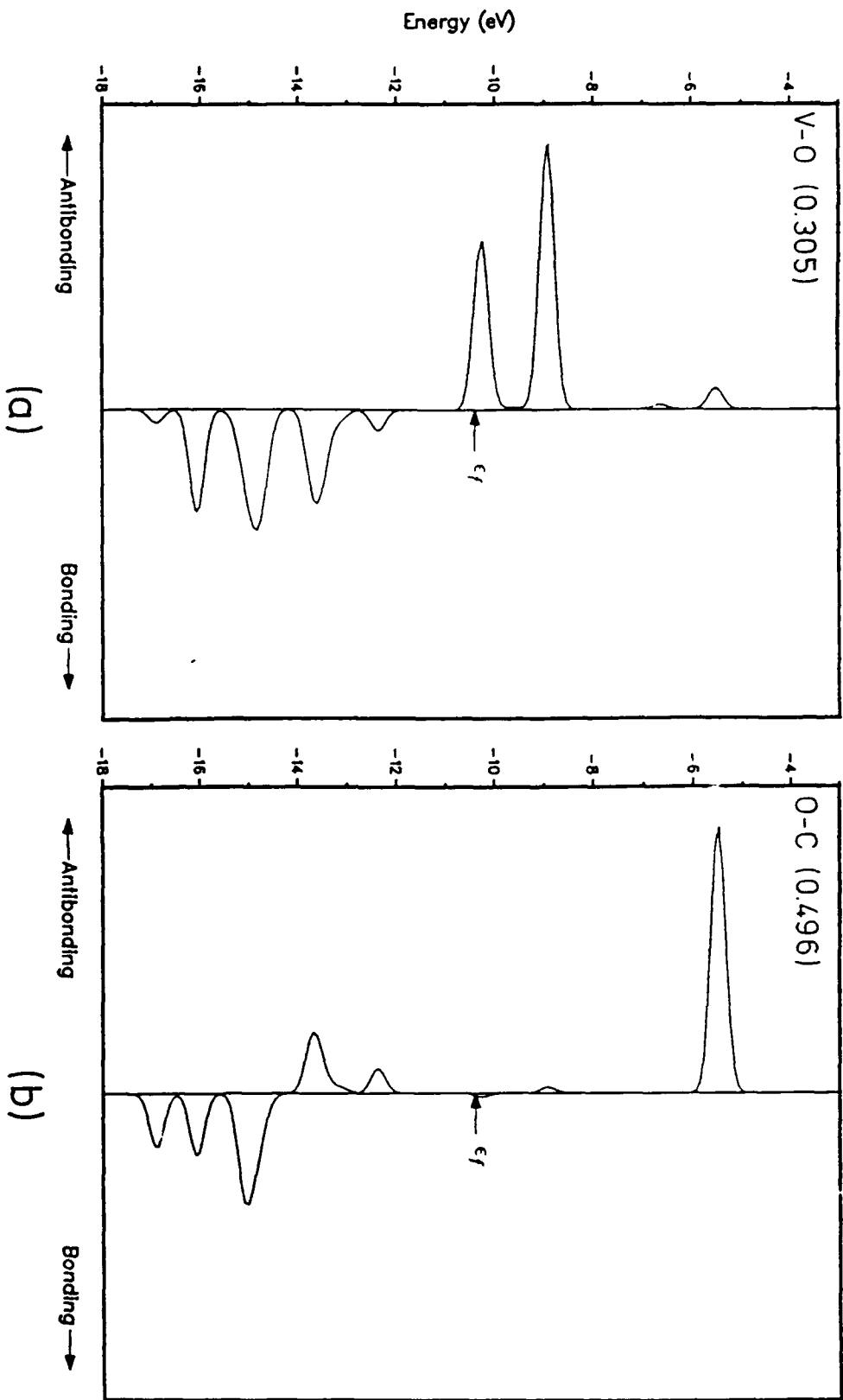
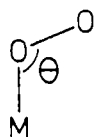


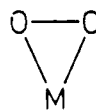
Figure 5: Some COOPs for the adsorption of DHF on the surface. (a) The COOP curve for the vanadium-oxygen double bond. (b) COOP for the carbon-oxygen bonds.

### The activation of O<sub>2</sub>(g) on the vanadyl pyrophosphate surface.

Bulk oxygens are not involved in the maleic anhydride formation from *n*-butane.<sup>7a,8</sup> Only lattice oxygens from the very outermost layers are transferred.<sup>8d</sup> The activation and incorporation of molecular oxygen into the vanadyl pyrophosphate surface is essential for keeping the large selectivity for maleic anhydride. Pepera *et al.*<sup>8a</sup> have showed that one oxygen molecule can be adsorbed per two surface vanadium centers. Within our model this could be one O<sub>2</sub> molecule per pair of edge-sharing vanadyl groups. An oxygen molecule can coordinate in two ways to one transition metal center,<sup>26</sup> as either a  $\eta^1$ -superoxo compound, 18, or in the  $\eta^2$ -coordinated (peroxo) way, 19. The bending angle,  $\Theta$ , of the known superoxo complexes varies from  $\sim 115^\circ$  to  $\sim 170^\circ$ .<sup>26</sup> Only structures with a

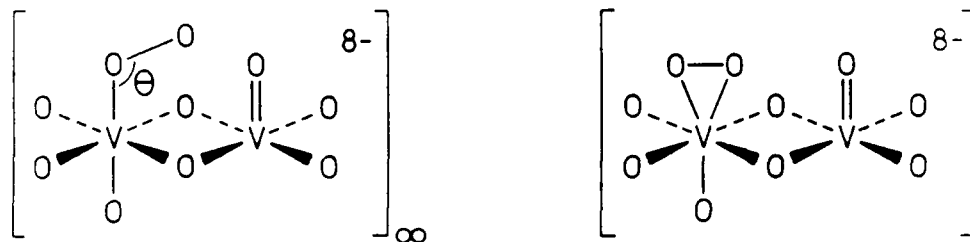


18



19

peroxo coordinated dioxygen has been reported for vanadium.<sup>27</sup> Table 4 contains some results for  $\eta^1$  and  $\eta^2$  coordinated dioxygen to a chain of (VO)<sub>2</sub>O<sub>6</sub><sup>8-</sup> units, 20. Three bending angles of the superoxo structure were used.



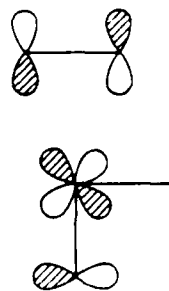
20

Table 4

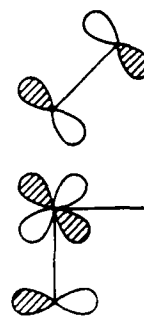
The separation of vanadium and one oxygen of the dioxygen fragment was taken to be 1.90 Å and the oxygen-oxygen distance to 1.40 Å.<sup>27</sup> A very flat minimum exists for the superoxo structure as a function of the bending angle,  $\Theta$ . The total energy is unchanged from 180° to ~150°. An angle of 90° is unfavorable by ~3 eV. The total energy of the peroxy form is only 0.5 eV higher than the superoxo form. An angle of 150° for **18** is applied in the rest of the study.

For both coordination modes a decrease in the oxygen-oxygen overlap population is calculated upon adsorption, from 0.570 in O<sub>2</sub>(g) to 0.395 and 0.413 for the  $\eta^1$  and  $\eta^2$  coordinated species, respectively. The vanadium to oxygen overlap population is highest in the peroxy structure.

The bond obtained between a  $\eta^2$  coordinated dioxygen and (VO)<sub>2</sub>O<sub>6</sub><sup>8-</sup> can be described as an interaction of the partly occupied  $\pi_z^*$  of O<sub>2</sub> and the unoccupied antibonding vanadium oxygen d<sub>xz</sub> + p<sub>x</sub> orbital, **21**. A gain of 0.12 electrons is calculated for d<sub>xz</sub>. For the superoxo structure the  $\sigma$  bond of O<sub>2</sub> is involved in bonding too. A loss of 0.11 electrons from the  $\sigma$  orbital is computed. This electron density is mainly transferred to d<sub>z2</sub> (0.06 electrons) and p<sub>z</sub> (0.08 electrons) of vanadium. Again, the  $\pi_z^*$  orbital of O<sub>2</sub> interacts with the antibonding d<sub>xz</sub> oxygen p<sub>x</sub> orbital, **22**.



21

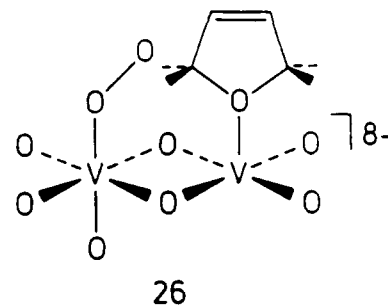
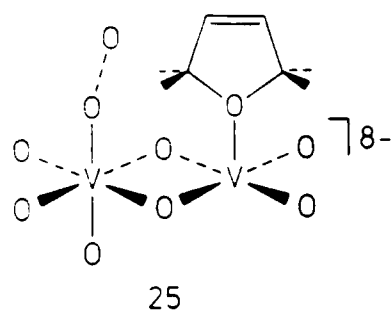
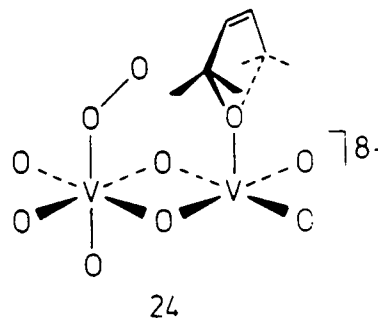
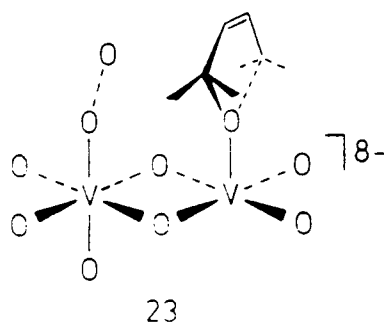


22

## Coadsorption of O<sub>2</sub>(g) and DHF on the vanadyl pyrophosphate surface.

### A model for the formation of maleic anhydride.

The presence of two vanadium atoms, located 3.19Å from each other, on the vanadyl pyrophosphate surface leads to a possible activation of O<sub>2</sub>(g) at one of the vanadium atoms, while DHF remains adsorbed at the other vanadium atom. There are four main combinations of a  $\eta^1$ -superoxo adsorbed molecular oxygen and DHF as outlined in 23 - 26.



For the coadsorption of  $\eta^2$ -peroxo molecular oxygen and DHF another four main possible orientations of O<sub>2</sub> and DHF emerge, as shown in 27 - 30.

Table 5 gives the total energy and some overlap populations of interest for the present study.

---

Table 5

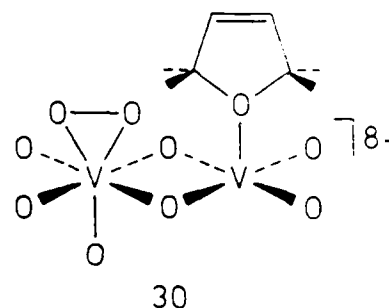
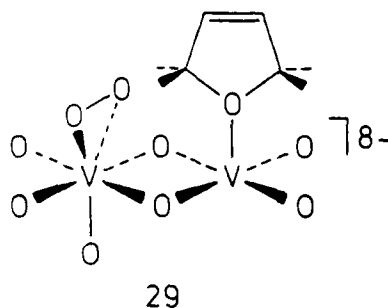
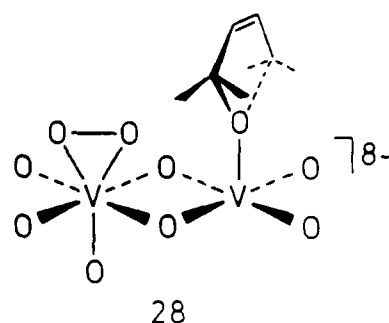
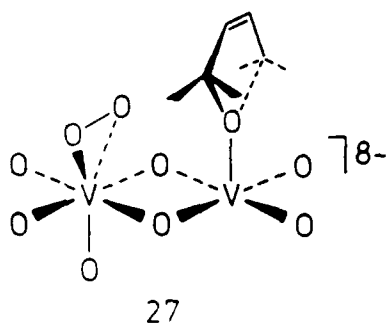
---

Table 4. Total energies and some overlap populations for 18 and 19.

	18	18	18	19
	$\theta = 180^\circ$	$\theta = 150^\circ$	$\theta = 90^\circ$	
Total energy	-1524.5 eV	-1524.7 eV	-1521.5 eV	-1524.2 eV
<u>Overlap populations</u>				
V = O <sup>a</sup>	0.720	0.721	0.721	0.697
O - O <sup>b</sup>	0.395	0.395	0.391	0.413

a: V=O overlap population for the vanadium atom with O<sub>2</sub> coordinated.

b: The O-O overlap population of O<sub>2</sub>(g) is 0.570



It appears from Table 5 that the energy difference is only 0.21 eV between the most stable structure with  $\eta^1$ -superoxo molecular oxygen coadsorbed with DHF on the vanadyl pyrophosphate surface and the lowest energy structure of  $\eta^2$ -peroxo molecular oxygen and DHF on the surface. This indicates that within the present calculational method it is not possible to distinguish between these two lowest energy structures of adsorbed molecular oxygen and DHF. In two other pairs of geometries of molecular oxygen and DHF coadsorbed (24 and 28, and 25 and 29) the difference in energy is also very small, whereas 26 is considerably higher in energy than 30. The latter case is due to electronic/steric repulsion between the terminal oxygen and the two hydrogens in the 2-position of DHF. The different overlap populations are remarkably constant for the different orientations of either a  $\eta^1$ -superoxo or a  $\eta^2$ -peroxo molecular oxygen coadsorbed with DHF. The only two overlap populations that are different

Table 5. Total energies, some overlap populations of 23 - 30 and the shortest O-H (H of DHF) distance.

	23	24	25	26	27	28	29	30
Energy (eV)	-1909.55	-1908.86	-1907.02	-1900.26	-1909.34	-1908.87	-1907.53	-1903.1
O-H (Å)	2.33	2.07	2.00	1.68	2.35	2.09	2.02	1.70
<u>Overlap Populations</u>								
V-O <sup>1</sup>	0.478	0.477	0.484	0.494	0.264	0.276	0.270	0.273
O-O <sup>2</sup>	0.396	0.397	0.402	0.399	0.416	0.415	0.416	0.400
O-H	0.000	0.000	0.000	-0.145	0.000	0.000	-0.030	-0.27
C-H	0.825	0.825	0.826	0.829	0.825	0.826	0.852	0.684

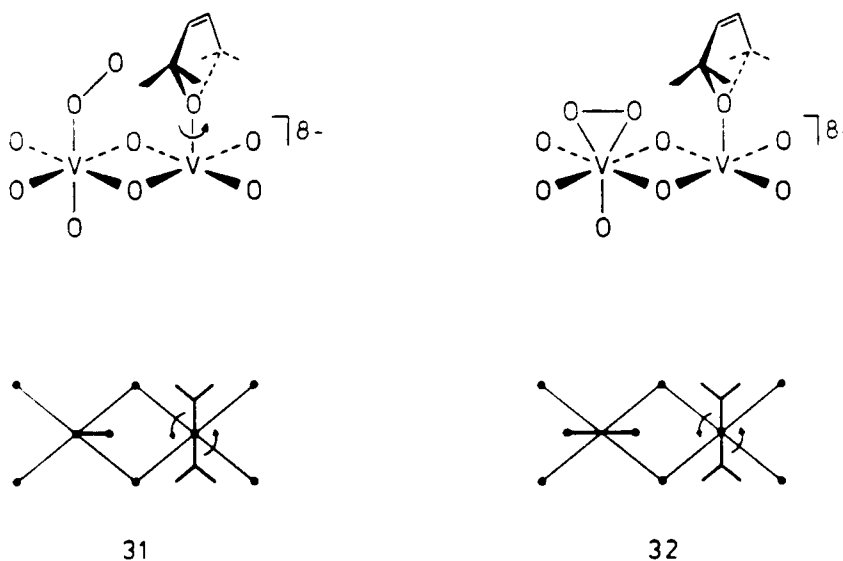
1: Oxygen of superoxo or peroxo (V-O: 1.90Å)

2: O-O: 1.40Å



for the various orientations are O-H or C-H in 26 and 30; a negative O-H overlap population is found in 26 and a reduction in the C-H overlap population is observed for 30.

We will now proceed to a description of how maleic anhydride can be formed from coadsorbed molecular oxygen and DHF on the vanadyl pyrophosphate surface. We are aware of the fact that the quantitative results obtained by the extended Hückel calculations cannot be sufficiently trusted in studies where several bonds are simultaneously formed or cleaved. But, as our intention, here in this part of the paper, is to give a qualitative description of the reaction path, this method should be able to provide us with some useful trends. As a starting point for our analysis we will study the rotation of DHF coadsorbed with either a superoxo or a peroxy molecular oxygen around the axes outlined in a topview in 31 and 32.



When rotating one of the two coadsorbed molecules on the vanadyl pyrophosphate surface the terminal oxygen of a  $\eta^1$ -superoxo or one of the oxygens in a  $\eta^2$ -peroxy adsorbed molecular oxygen is brought close to the hydrogen of the C-H bond in the 2-position at DHF. These approaches of oxygen to hydrogen leads to several electronic changes.

In the rotation DHF starts out being oriented perpendicular to the V-V direction of the surface whereas the oxygen fragment, either superoxo or peroxy, stays fixed along the V-V direction (31 and 32). Figure 6 shows the

changes in energy for the two different systems as a function of the O-H distance. The rotations shown correspond to rotation angles from 0° to 75° round the V-O (DHF) axis.

---

Figure 6

---

From Figure 6 it is seen that in the course of the rotation of DHF, when coadsorbed with a peroxo species, the approach of the hydrogen in DHF leads to an increase in energy. It costs about 4.6 eV to rotate. In the superoxo case about 6.8 eV is required for the approach of the hydrogen to oxygen to the same O-H distance (1.15 Å), which indicates that the former is the least unfavorable. Besides the changes in energy several changes in bonding is also observed: For the rotation 31 the C-H overlap population in DHF is reduced from 0.826 to 0.525, whereas the O-H overlap population increases from 0.000 to 0.209 over the range the O-H bond distances in Figure 6. This tells us that the C-H bond is weakened and that a O-H bond is made. The V-O (the oxygen which interacts with the hydrogen) overlap population in 32 is also affected by the rotation; it decreases from 0.281 to 0.234. In rotation 32 the C-H overlap population of DHF is also reduced from 0.826 to 0.286, whereas the O-H overlap population again shows an increase from 0.000 to 0.408 for the O-H bond distance changes of Figure 6. This also indicates a weakening of the C-H bond and an O-H bond being formed too.

The change in nature of the C-H bond of DHF and of the interaction between an oxygen from the peroxo fragment and hydrogen in DHF can be traced to a controlling orbital interaction; the  $\sigma_{\text{C-H}}$  donates electron density into the  $\sigma_{\text{O-O}}^*$  orbital which is the LUMO of the peroxo group that is coordinated to vanadium as shown in 33. The  $\sigma_{\text{C-H}}$  orbital donates 0.3 electrons into the  $\sigma_{\text{O-O}}^*$  orbital by this interaction.

The donation of electron density from the  $\sigma_{\text{C-H}}$  orbital into the  $\sigma_{\text{O-O}}^*$  orbital thus leads to the weakening/cleavage of the C-H bond and the formation of an O-H bond. A similar type of C-H activation has also been found in the reactions of several types of transition-metal peroxo

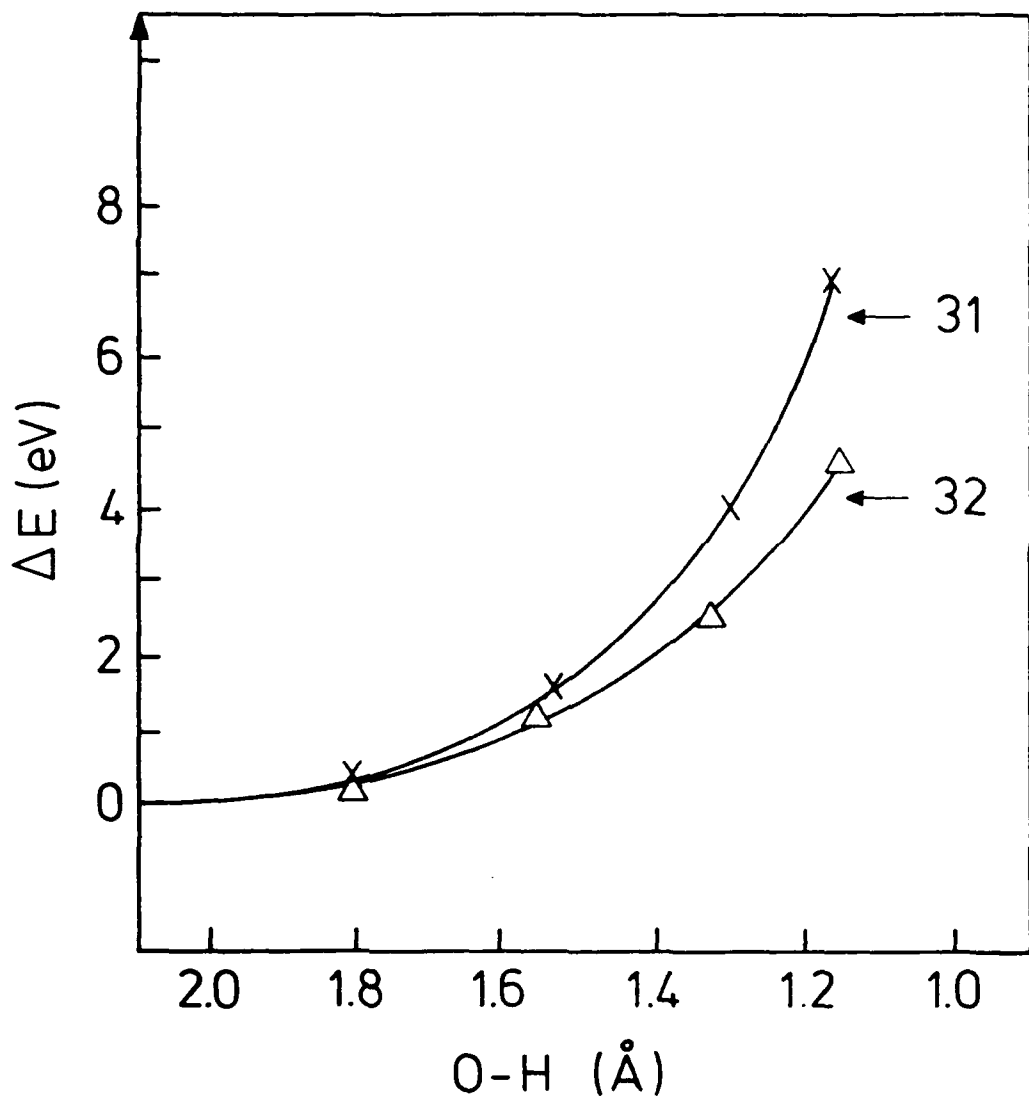
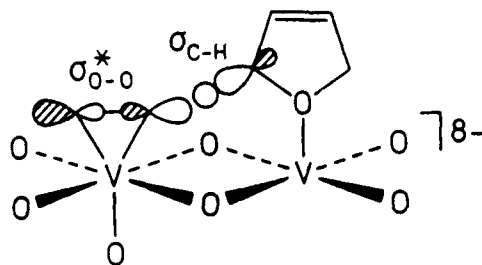


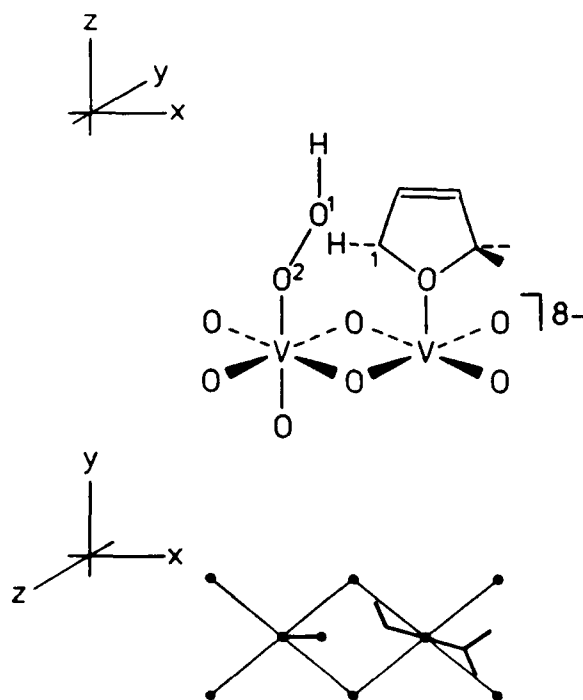
Figure 6: Variation in the total energy of 31 and 32 when rotating around the V-O (DHF) axis. The O-H distance is measured from the hydrogen in the 2-position of DHF to the nearest oxygen located at the adjacent vanadium atom.

complexes;<sup>28</sup> in the case of transition-metal peroxo complexes the reaction with *e.g.* benzene leads to a hydroxylation reaction.<sup>28</sup>



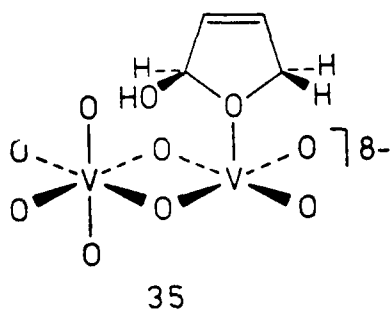
33

The first step of this proposed mechanism causes a hydrogen transfer from the 2-position in DHF to, probably, one of the oxygens of a coadsorbed  $\eta^2$ -peroxo oxygen fragment, although we can not, on the basis of these calculations, exclude the  $\eta^1$ -superoxo species being active in the process. When an oxygen from the  $\eta^2$ -peroxo species interacts with the hydrogen the observed decrease in overlap population for the V-O bond (O from  $\eta^2$ -peroxo) might indicate the this bond will break by the hydrogen transfer reaction, leading to a  $\eta^1$  coordinated O-O-H as shown in 34. The same intermediate is also formed in the case of an interaction between a  $\eta^1$ -superoxo dioxygen coadsorbed with DHF.



34

Calculation of the preferred orientation of the O-H group in **34** shows that an orientation with the hydrogen pointing in the z-direction is 0.24 eV more favorable than the one where the hydrogen points in the opposite direction. With **34** as intermediate on the reaction path the formation of the 2-hydroxy derivative of DHF is a feasible process. The orientation of DHF, for which the hydrogen is transferred to the oxygen, is also the optimum position for interaction between O<sup>1</sup> and C<sup>1</sup> of **34**. In this position the C<sup>1</sup>-O<sup>1</sup> overlap population is 0.635 (C<sup>1</sup>-O<sup>1</sup> distance 1.60 Å) showing that significant C-O bonding is present. If the DHF derivative in **34** is rotated away from this optimum position ( with the DHF derivative rotated 15° away from the V-V direction) to e.g. a position where the DHF derivative is oriented perpendicular to this direction, the energy required for bringing it back to the optimum position is less than 2 eV. Besides the formation of a C-O bond the O<sup>1</sup>-O<sup>2</sup> overlap population is also reduced slightly when C<sup>1</sup> and O<sup>1</sup> interacts. With the DHF derivative oriented perpendicular to the V-V direction the O<sup>1</sup>-O<sup>2</sup> overlap population is 0.420, and 0.401 in the position where the optimum interaction between C<sup>1</sup>-O<sup>1</sup> occurs. The process described here gives then the 2-hydroxy derivative of DHF (2HDHF) and an adjacent V-O function on the surface, **35**.



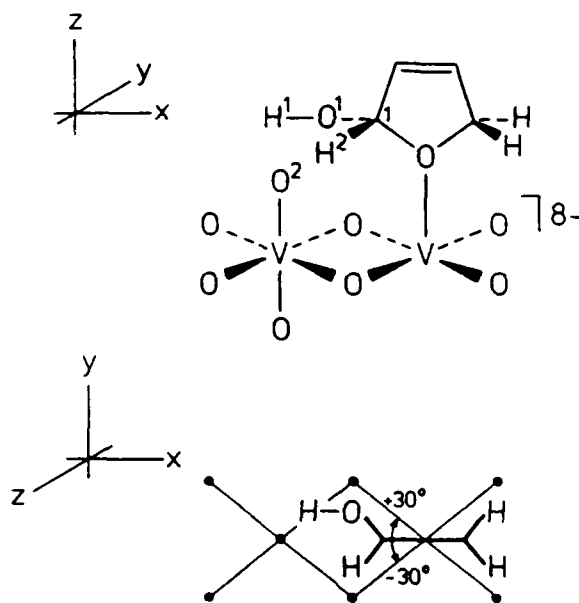
The above description of the formation of **35** is a two-step process, but we can not exclude a one-step process, an "attachment-insertion" reaction similar to the one suggested for the hydroxylation of C-H bonds by oxene-like reagents.<sup>29</sup>

The presence of the V-O function adjacent to 2HDHF is also important

for the further reaction. The V-O function is located in an optimum position for interaction with the hydroxy function in 2HDHF, leading to the asymmetric unsaturated lactone. The electronic structure of the V-O function can be established from the frontier orbitals of 35 shown in Figure 7.

Figure 7

Figure 7 shows that the V-O function contributes to the frontier orbitals with low lying unoccupied as well as with relatively high lying occupied molecular orbitals of both  $p_x$ ,  $p_y$  and  $p_z$  character. These orbitals then have the possibility of interacting with either the O-H or C-H bond in 2HDHF by accepting or donating electron density. The interaction of the O-H and the C-H bond in 2HDHF is analyzed as a function of the rotation angle of 2HDHF, going from  $-30^\circ$  to  $+30^\circ$ , as shown in 36, in an attempt to elucidate the next step in the formation of the asymmetric unsaturated lactone.



36

In the rotation sketched in 36, the shortest  $H^1-O^2$  distance is 1.17 Å and the shortest  $H^2-O^2$  is 1.61 Å, indicating that the best interaction between 2HDHF and the oxygen on the adjacent vanadium atom is the interaction

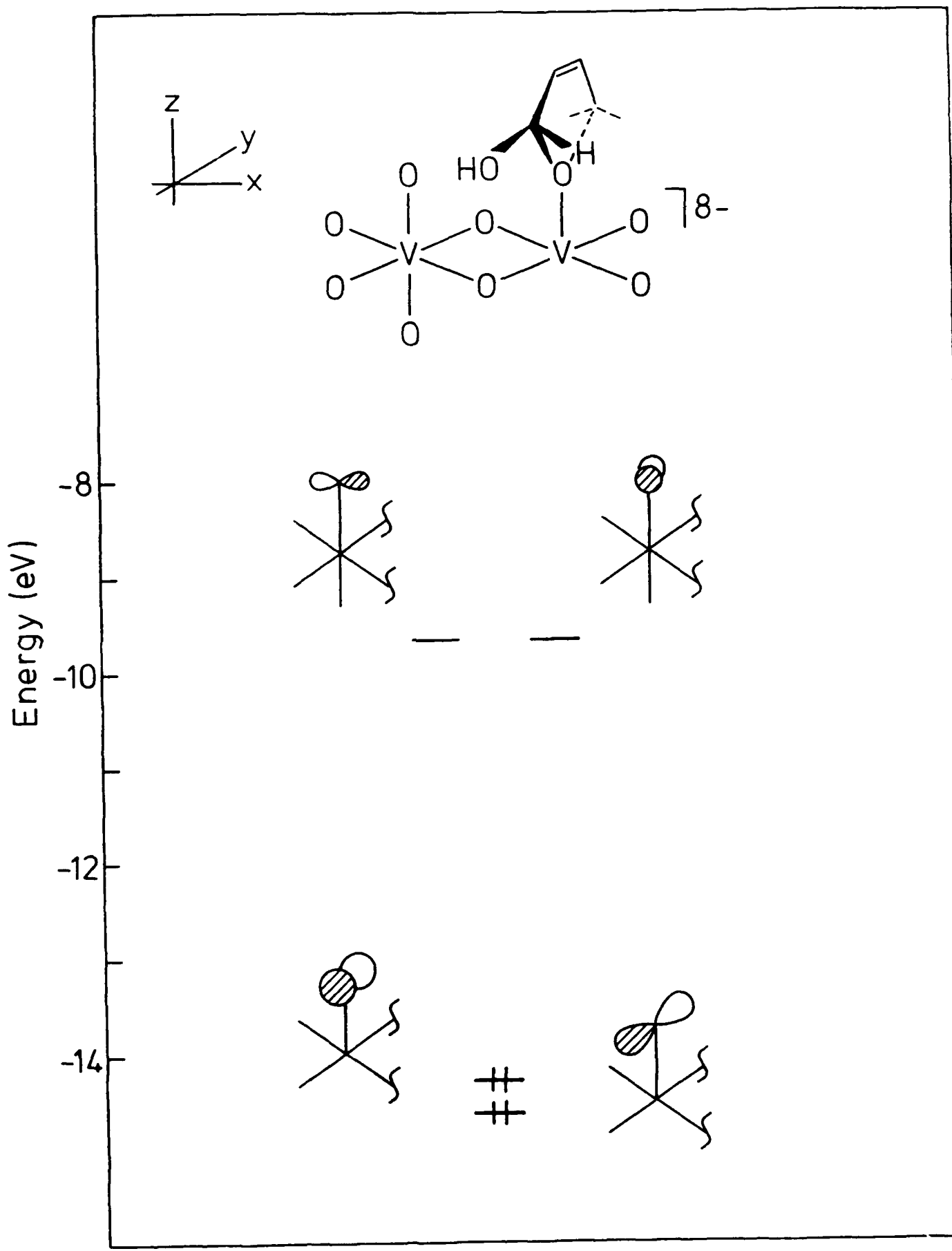
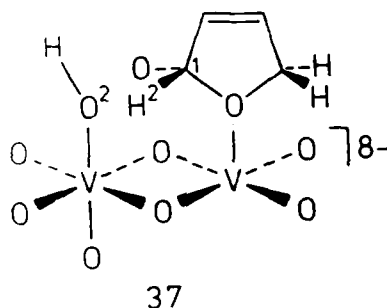


Figure 7: The frontier orbitals of the vanadium-oxygen bond in 35.

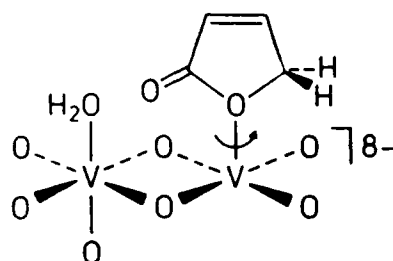
of  $O^2$  with the  $H^1$  of the hydroxyl group of 2HDHF. The total energy of the system rises by about 2 eV upon a rotation of  $+30^\circ$ . Several electronic changes take place upon rotation: The  $H^1-O^2$  distance is 1.78 Å in the starting position with the following overlap populations:  $C^1-O^1$  0.601,  $O^1-H^1$  0.603 and  $H^1-O^2$  -0.02; in the position with the shortest  $H^1-O^2$  distance (1.17 Å) these overlap populations have changed to: 0.633, 0.366 and 0.154, respectively. These results show that when the  $C^1-O^1$  bond increases in strength, meaning that the  $C=O$  bond is beginning to form, the  $O^1-H^1$  bond is weakened and a  $H^1-O^2$  bond is being formed. The formation of  $H^1-O^2$  bond can be traced to interaction between the second HOMO shown in Figure 7 and the  $\sigma^*_{O-H}$  in the hydroxyl group in 2HDHF.

By the reaction path presented so far we are now near the end of the reaction, for we have reached a hydroxy group at the adjacent vanadium atom and a 2HDHF radical-like species coordinated to the other vanadium atom, as shown in 37.



With an orientation of the system as depicted in 37, the last step in the formation of the asymmetric unsaturated lactone is an abstraction and a transfer of  $H^2$  to  $O^2$ , and a rehybridization of  $C^1$  from  $sp^3$  to  $sp^2$ . The  $H^2-O^2$  distance in 37, with the bond lengths and angles used here for the adsorbed species (see Appendix) is calculated to be 1.61 Å, and for this distance a small  $H^2-O^2$  overlap population is observed (0.06), indicating that a hydrogen transfer might be possible. This transfer of  $H^2$  to  $O^2$ , under formation of  $H_2O$  and the asymmetric unsaturated lactone, 38, leads to a decrease in the total energy of the system by 0.87 eV, also showing that the process seems possible.





38

By the process described so far DHF has by use of one molecular oxygen been oxidized to the asymmetric unsaturated lactone and a water molecule on the vanadyl pyrophosphate surface. The next step in the formation of maleic anhydride on the vanadyl pyrophosphate surface is an exchange of the water molecule with molecular oxygen in 38 and a rotation of the asymmetric unsaturated lactone by  $180^\circ$ . This would lead another  $\text{CH}_2$  group to be near the newly adsorbed and activated molecular dioxygen at the adjacent vanadium atom. The formation of maleic anhydride can thus take place in a way similar to that described above for the formation the asymmetric unsaturated lactone. The present results seem to support the observation by Busca and Centi, that the lower reaction path of Scheme 1 represents a likely path for the formation of maleic anhydride on a vanadyl pyrophosphate surface.

## Conclusion.

In this study we have analysed the electronic structure of the vanadyl pyrophosphate surface trying to explain some of the steps involved in the transformation of *n*-butane to maleic anhydride catalyzed by this surface using molecular oxygen as the oxygen donor. First, an electrophilic oxygen from a surface vanadyl group can insert in the 1,4-positions of butadiene in a concerted [2+4] like cycloaddition process. The thereby formed 2,5-dihydrofuran fragment rearranges itself to a "vertical" position where it can interact with a neighbouring adsorbed dioxygen species.

The nature of this dioxygen fragment when adsorbed on a clean vanadyl pyrophosphate surface was analyzed. The two coordination modes,  $\eta^1$  ( $\Theta = 150^\circ$ ) and  $\eta^2$ , gave quite similar results, so a definite assignment of the geometry could not be made. When interacting with a coadsorbed DHF molecule the  $\eta^2$ -peroxo form seems to provide the most likely structure of the dioxygen part, but the  $\eta^1$ -superoxo possibility cannot be excluded. Both dioxygen structures upon abstraction of an  $\alpha$ -hydrogen from DHF lead to an O-O-H surface species. This species can transfer an OH group to the DHF radical derivative forming a new vanadyl group. The newly formed hydroxylated DHF can eliminate water upon reaction with the new neighbouring vanadyl oxygen leaving back, on the surface, the asymmetric unsaturated lactone. Another molecule of O<sub>2</sub> can undergo the exactly same reaction sequence with the  $\beta$ -position of the lactone. More detailed mechanistic studies of these later steps of the proposed reaction path will definitely be of great interest.

## Acknowledgement.

B. S. is thankful to the Carlsberg Foundation for economical support and to Thanks to Scandinavia, Inc. (especially Mr. Richard Netter) for making a stay at Cornell possible. We are thankful to Arne Lindahl for his carefully preparation of the drawings and to Susan Jansen for sending a paper prior to publication.

Table 6: Atomic parameters.

Atom	Orbital	$H_{II}^i$ (eV)	$\xi_1$	$\xi_2$	$c_1^a$	$c_2^a$
V	4s	-8.81	1.30			
	4p	-5.52	1.30			
O	3d	-11.00	4.75	1.70	0.4755	0.7052
	2s	-32.20	2.28			
	2p	-14.80	2.28			
	2s	-21.40	1.63			
C	2s	-21.40	1.63			
	2p	-11.40	1.63			
H	1s	-13.60	1.30			

a: Coefficients used in the double zeta expansion of the metal d-orbitals.

## Appendix.

The extended Hückel<sup>19</sup> molecular and tight binding<sup>20</sup> approach is applied throughout this study. Bond distances and angles for the different surface models are taken as average of the experimental values reported for the vanadyl pyrophosphate structure.<sup>12</sup> This leads to a V-V distance of 3.188Å and a V=O distance of 1.628Å. The geometry of 2,5-dihydrofuran is in accordance with the experimentally reported structure.<sup>30</sup> Butadiene has C-C separations of 1.48Å and 1.34Å and all angles are 120°. <sup>31</sup> The dioxygen species have an O-O distance of 1.40Å.<sup>26</sup> The distance between vanadium and an oxygen from the adsorbed dioxygen is 1.90Å.<sup>25</sup> Atomic parameters are listed in Table 6. In the tight binding calculations properties averaged over the Brillouin zone were estimated by the use of a 10 *k*-point set according to the geometrical method by Ramirez and Böhm.<sup>32</sup>

---

Table 6

---

## References:

1. a) Sheldon, R. A.; Kochi J. A. "Metal Catalyzed Oxidations of Organic Compounds" Academic Press, New York, 1981.  
b) Holm, R. *Chem. Rev.* 1987, 87, 1401.  
c) Jørgensen, K. A. *Chem. Rev.* 1989, 89, 431.  
d) Nugent, W. A.; Mayer, J. M. "Metal-Ligand Multiple Bonds" Wiley Interscience, New York, 1988.  
e) Meunier, B.; *Bull. Soc. Chim. Fr.* 1986, 578.
2. a) Burrington, J. D.; Grasselli, R. K. *J. Catal.* 1979, 59, 79;  
b) Burrington, J. D.; Kartisek, C. T. Grasselli, R. K. *J. Catal.* 1980, 63, 253; *ibid* 1983, 81, 489; *ibid* 1984, 87, 363.  
c) Otamiri, J.; Anderson, A.; Jansen, S. A. *Langmuir* 1990, xx, xxx.
3. Grasselli, R. K. *J. Chem. Educ.* 1986, 63, 216.
4. a) Barteau, M. A.; Madix, R. J. in "The Chemical Physics of Solid Surfaces and Heterogeneous Catalysis" (ed) King, D. A.; Woodruff, D. P. Elsevier Scientific Publishing Company, 1982, 95.  
b) van Santen, R. A.; Kuipers, H. P. C. E.; *Adv. Catal.* 1989, 35, 265.
5. Anderson, A. B.; Ewing, D. W.; Kim, Y.; Grasselli, R. K.; Burrington, J. D.; Brazdil, J. F. *J. Catal.* 1985, 96, 222.
6. a) Carter, E. A.; Goddard III, W. A. *J. Catal.* 1988, 112, 80; *Surf. Sci.* 1989, 209, 243.  
b) Jørgensen, K. A.; Hoffmann, R. *J. Phys. Chem.* 1990, xx, xxx.
7. a) Centi, G.; Trifirò, F.; Ebner, J. R.; Franchetti, V. M. *Chem. Rev.* 1988, 88, 55.  
b) Hodnett, B. K. *Catal. Rev.-Sci. Eng.* 1985, 27, 373.
8. a) Pepera, M. A.; Callahan, J. L.; Desmond, M. J.; Milberger E. C.; Blum, P. R.; Bremer, N. J. *J. Am. Chem. Soc.* 1985, 107, 4883.  
b) Busca, G.; Centi, G. *J. Am. Chem. Soc.* 1989, 111, 46.  
c) Wohlfahrt, K.; Hofmann, H. *Chem.-Ing.-Tech.* 1980, 52, 811.  
d) Kruchinin, Yu. A.; Mishchenko, Yu. A.; Nechiporuk, P. P.; Gel'bshtein, A. I. *Kinet. Katal. (Engl. Transl.)* 1984, 25, 328.
9. a) Tachez, M.; Theobald, F.; Bordes, E. J. *Solid State Chem.*

- 1981, 40, 280.
- b) Torardi, C. C.; Calabrese, J. C. *Inorg. Chem.* 1984, 23, 1308.
- c) Bordes, E.; Courtine, P. *J. Chem. Soc., Chem. Commun.* 1985, 294.
- d) Bordes, E.; Johnson, J.W.; Ramonosona, A.; Courtine, P.; "Proceedings of the 10th International Symposium on the Reactivity of Solids" (Dijon, 1984), Matr. Sci. Monogr. 28B, 887.
10. a) Johnson, J. W.; Johnston, D. C.; Jacobson, A. J.; Brody, J. F. *J. Am. Chem. Soc.* 1984, 106, 8123.
11. a) Bordes, E.; Courtine, P. *J. Catal.* 1979, 57, 236.
- b) Cavani, F.; Centi, G.; Trifirò, F. *Appl. Catal.* 1984, 9, 191.
- c) Centi, G.; Manenti, I.; Riva, A.; Trifirò, F. *Appl. Catal.* 1984, 9, 177.
- d) Johnston, D. C.; Johnson, J. W. *J. Chem. Soc., Chem. Commun.* 1985, 1720.
12. Gorbunova, Yu. E.; Linde, S. A. *Sov. Phys. Dokl. (Engl. Transl.)* 1979, 24, 138.
13. Satsuma, A.; Hattori, A.; Furuta, A.; Miyamota, A.; Hattori, T.; Murakami, Y. *J. Phys. Chem.* 1988, 92, 2275.
14. Busca, G.; Centi, G.; Trifirò, F. *Appl. Catal.* 1986, 25, 265.
15. a) Centi, G.; Trifirò, F. *J. Mol. Catal.* 1986, 35, 255.
- b) Morselli, L.; Trifirò, F.; Urban, L. *J. Catal.* 1982, 75, 112.
16. a) Krenzke, L. D.; Keulks, G. W. *J. Catal.* 1980, 61, 316.
- b) Brazdil, J. F.; Suresh, D. D.; Grasselli, R. K. *J. Catal.* 1980, 66, 347.
- c) Glaeser, L. C.; Brazdil, J. F.; Hazle, M. A.; Mehecić, M.; Grasselli, R. K. *J. Chem. Soc., Faraday Trans. I* 1985, 81, 2903.
- d) Mars, P.; van Krevelen, D. W. *Chem. Eng. Sci. (Spec. Suppl.)* 1954, 3 41.
17. Ueda, W.; Moro-oka, Y.; Ikawa, T. *J. Chem. Soc., Faraday Trans. I* 1982, 78, 495.
18. Buchanan, J. S.; Sundrasan, S. *Appl. Catal.* 1986, 26, 211.

19. a) Hoffmann, R. *J. Chem. Phys.* **1963**, *39*, 1397.  
b) Hoffmann, R.; Lipscomb, W. N. *J. Chem. Phys.* **1962**, *37*, 2872.
20. Whangbo, M.-H.; Hoffmann, R. *J. Am. Chem. Soc.* **1978**, *100*, 6093.
21. Saillard, J.-Y.; Hoffmann, R. *J. Am. Chem. Soc.* **1984**, *106*, 2006.
22. Halet, J.-F.; Hoffmann, R. *J. Am. Chem. Soc.* **1989**, *111*, 3548.
23. Cavani, F.; Centi, G.; Trifirò, F. *Appl. Catal.* **1985**, *15*, 157.
24. a) Hoffmann, R. *"Solids and Surfaces. A Chemists View of Bonding in Extended Structures."* VCH Publishers, Inc. New York **1988**.  
b) Hoffmann, R. *Rev. Mod. Phys.* **1988**, *60*, 601.  
c) Hoffmann, R. *Angew. Chem., Int. Ed. Engl.* **1987**, *26*, 846.
25. Mimoun, H.; Chaumette, P.; Mignard, M.; Saussine, L. *New. J. Chem.* **1983**, *7*, 467.
26. Gubelmann, M. H.; Williams, A. F.; *"The Structure and Reactivity of Dioxygen Complexes of the Transition Metals"* in *"Structure and Bonding"* VCH Publishers **1984**, *1*.
27. a) Svensson, I.-B.; Stomberg, R. *Acta. Chem. Scand.* **1971**, *25*, 898.  
b) Drew, R. E.; Einstein, F. W. B. *Inorg. Chem.* **1972**, *11*, 1079; *ibid* **1973**, *12*, 829.  
c) Mimoun, H. in *"The Chemistry of Peroxides"* (Ed. Patai, S.) Wiley Interscience **1983**, New York.
28. See e.g. Bonchio, M.; Conte, V.; Di Furia, F.; Modena, G. *J. Org. Chem.* **1989**, *54*, 4368.
29. Korzekwa, K.; Trager, W.; Gouterman, M.; Spangler, D.; Loew, G.; *J. Am. Chem. Soc.* **1985**, *107*, 4273.
30. Courtieu, J.; Gounelle, Y. *Mol. Phys.* **1974**, *28*, 161.
31. March, J. *"Advanced Organic Chemistry"* 3<sup>rd</sup> ed. Wiley Interscience **1985** New York, p. 19.

32. Ramirez, R.; Böhm, M. C. *Int. Quantum, Chem.* 1986, 30, 391.